TRB

TRANSPORTATION RESEARCH RECORD

l of the Transportation Research Board, No. 1929

Bituminous Paving Mixtures 2005

Transportation Research Record 1929

Contents

Effect of Construction Quality, Temperature, and Rutting on Initiation of Top-Down Cracking

Elisabete Fraga de Freitas, Paulo Pereira, Luis Picado-Santos, and A. Thomas Papagiannakis

Top-down cracking (TDC) is a flexible pavement distress caused by a number of factors, including high contact stresses from truck tires, mix design characteristics (e.g., binder type and aggregate gradation), and poor construction quality (e.g., segregation and compaction methods). This paper presents the findings of a study seeking to quantify the effect of those factors on TDC. The study consists of a laboratory component involving an accelerated wheel-tracking device and a modeling component involving a 3-D nonlinear viscoelastic finite element model. The laboratory component of the study involved 17 asphalt bituminous slabs constructed to simulate the variation in material properties observed in the field as part of an earlier forensic TDC study. The effect on TDC of air voids, bitumen content and type, aggregate gradation, and segregation were studied under three temperature conditions. Air voids, segregation, and binder content were found to have a significant effect on TDC for all temperatures tested. Modeling the TDC involved laboratory testing to establish the viscoelastic and tensile strength properties of the asphalt mixtures tested. It was found that the rutted surface contributes significantly to TDC initiation.

Top-down cracking (TDC) is a flexible pavement distress defined by cracks beginning at the surface of the asphalt concrete layer and propagating downward with time. TDC has received relatively little attention in the literature compared with the so-called conventional traffic-associated flexible pavement distresses, such as bottom-up asphalt concrete cracking and granular layer rutting. Recently, there has been renewed interest in modeling the initiation and progression of TDC (e.g., the new pavement design guide being developed by NCHRP Study 1-37A and the ongoing NCHRP Study 1-42). Clearly, TDC is a distress mechanism that needs to be better understood, incorporated into pavement performance prediction models, and included in the systems used for managing pavements.

The literature suggests that TDC begins in the first few years of pavement life, for example, in the first year as reported in Japan (*1*), although it could begin much later, for example, in the 10th year, as reported in Florida (*2*). It appears to occur in a variety of asphalt concrete pavements located in a wide range of environmental conditions. Cracks appear mainly outside the wheel path, in areas exposed to extensive solar radiation (*2–4*). Six main factors have been reported to contribute to TDC initiation and propagation:

- Climatic conditions (*3, 5*);
- Traffic conditions, including the load and inflation pressure of truck tires (*2, 6, 7*);
- Aging of the binder (*8*);
- Structural conditions, including layer thickness (*3, 9, 10*);
- Mixture properties, including binder type and aggregate gradation (*1*); and
- Construction quality, including segregation and compaction procedures (*9–12*).

Nevertheless, the cause–effect relationship between each of these factors, their interaction, and TDC is not clearly understood. Preliminary work for this study involved forensic analysis of eight 80- × 80- × 30-cm asphalt slabs and 44 cores extracted from an 8-year-old roadway pavement in the north of Portugal revealing TDC (*4*). Physical examination of these field samples revealed construction quality, mainly in the form of segregation, as the main cause of TDC initiation and progression. That was evident not only in the wearing course but also in the leveling courses. Aggregates were poorly graded and exhibited excessive fine particles. Void content was high and showed a large variability in each slab. Bitumen content was, on average, slightly higher than 6%. Additional in situ deflection measurements were obtained in the spring with a falling weight deflectometer. They revealed no structural deficiencies for the traffic level at the site, that is, maximum deflections were lower than 300 μm. Samples from the wearing course were further tested in the laboratory, involving a repetitive constant height simple shear tester (SST) (*11*). The stiffness modulus was found to be higher than 4,500 MPa at 20°C and 10 Hz; the phase angle was lower than 10°, suggesting significant stiffening of the wearing course through aging. A significant reduction in modulus was observed by increasing temperature from 10°C to 25°C. These results provided a guideline for selecting variables to include in further evaluation of TDC initiation, as described below.

OBJECTIVE METHODOLOGY

The objective of the part of the study reported here is to further evaluate the effect of the factors identified above on TDC initiation. Factors include binder type, binder content, aggregate gradation, void content, aggregate–binder adhesion, and temperature. This part of the study includes a laboratory component using a wheel-tracking device and a modeling component using a nonlinear viscoelastic finite element model.

E. F. Freitas and P. Pereira, Department of Civil Engineering, University of Minho, Campus de Azurém, 4800 058 Guimarães, Portugal. L. Picado-Santos, Department of Civil Engineering, University of Coimbra, Pinhal de Marrocos, 3030 290 Coimbra, Portugal. A. T. Papagiannakis, Department of Civil and Environmental Engineering, Washington State University, Pullman WA, 99164-2910.

Transportation Research Record: Journal of the Transportation Research Board, No. 1929, Transportation Research Board of the National Academies, Washington, D.C., 2005, pp. 174–182.

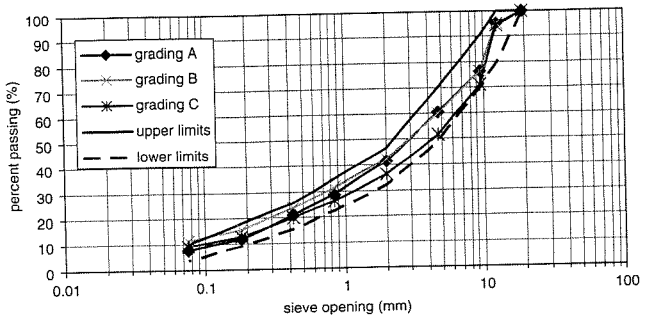

FIGURE 1 Grading curves and grading envelope.

The laboratory component involved manufacturing 17 asphalt concrete slabs with the goal of replicating the range of conditions encountered in the field during the forensic analysis conducted earlier. Mixture design took into account project specifications and field quality control, as well as possible mitigation measures. A 50/70 penetration binder was used. Granite aggregates were used, and limestone filler was added to the aggregate blend, in the necessary proportion, to obtain the three grading curves depicted in Figure 1. Curve A approaches the grading envelope average curve recommended in the field study. Curves B and C are, respectively, fine graded and coarse graded, approaching the upper and lower gradation limits of the field specification. Three levels of binder content and air voids were considered (i.e., high, normal, and low) within ranges found in the preliminary work. Control binder content was set at 5.8% according to the Duriez model and the field tests previously performed (*13*). Control void content was set at 4% according to project specifications. The segregation observed in the field was also simulated in the laboratory mixtures. Two additional mixtures were produced, one with hard bitumen and another using an antistripping compound. These mixtures were compacted in a 75.0- × 55.0- × 7.0-cm rectangular mold using a vibratory roller compacter. Specimens were obtained by cutting them from the slabs produced in the laboratory with the required dimension. A summary of each slab's physical properties, as well as testing temperature, is presented in Table 1. Testing temperatures were selected to be representative of the range in wearing course daily temperatures measured in the summer in the north of Portugal.

The modeling component of the study involved a nonlinear viscoelastic finite element algorithm. A number of additional laboratory tests were conducted to obtain the material properties required for modeling. These included stiffness, shear modulus, and tensile strength of the asphalt concrete. In addition, cyclic compression tests were performed to model the viscoelastic behavior of the asphalt concrete at high temperatures.

WHEEL-TRACKING TEST

There have been several studies in the literature dealing with TDC using accelerated loading devices. Groenendijk used the accelerated loading facility LINTRACK to observe TDC behavior (*6*). The Public Works Research Institute of Japan custom-developed a testing machine to evaluate the effect of mixture characteristics on TDC (*1*). Uchida et al. (*8*) and Wang et al. (*14*) used a device similar to the wheel-tracking test apparatus. The former studied the effect of aging

TABLE 1 Slab Characteristics

Parameter	Slab Number																
	1	2	3	4	5	6	7	8	9	10	11	12	13	14	15	16	17
Grading (A, B, C)	A	A	A	B	C	A	A	A	A	A	B	C	A	A	A	A	A
Density (g/cm³)	2.24	2.32	2.34	2.33	2.31	2.30	2.26	2.32	2.29	2.31	2.30	2.30	2.30	2.30	2.31	2.27	2.24
Void content (%)	8.2	4.1	2.1	4.1	4.6	5.6	7.8	4.1	4.4	3.8	3.2	4.9	4.6	3.8	4.2	6.6	7.8
Bitumen content (%)	5.7	5.8	7.6	6.1	5.8	5.8	5.3	5.7	5.8	5.8	6.1	5.8	5.8	5.8	5.3	5.8	5.8
Bitumen type (1:50/70; 2:35/50)	1	1	1	1	1	1	1	1	1	1	1	1	1	1	1	2	1
Additive (‰)	0	0	0	0	0	0	0	0	0	0	0	0	0	0	0	0	3
Segregation (yes, no)	No	No	No	No	No	No	No	No	No	No	No	No	Yes	Yes	No	No	Yes
Temperature (°C)	50	50	50	50	50	50	50	30	50	40	30	40	50	30	40	50	50

on TDC initiation, and the latter studied TDC initiation of the deformed specimens from a micromechanics perspective.

In this study a wheel-tracking test apparatus was used. It is recognized that this device does not realistically replicate the horizontal contact stresses applied by tires at the surface of a pavement. That is an inherent limitation of using the device, especially because these stresses are reported in the literature as one of the main causes of TDC (2). Another variable not considered in this test is the effect of binder aging and the resulting increase in the stiffness of the asphalt concrete.

A steel mold has been used to provide confinement to the 30.5- × 30.5- × 7.0-cm specimens. The specimens were subjected to a 0.69-kN wheel load, which corresponds to a 627-kPa pressure, traveling back and forth along the center line. The contact area was 4.9 × 2.2 cm^2, and the loading period was 1.395 s. Testing was conducted at three temperatures, namely, 30°C, 40°C, and 50°C (Table 1). The condition of the surface was monitored closely to identify the number of cycles that correspond to the initiation of surface cracks. Furthermore, the rut depth was recorded as a function of the number of axle passes. Testing was terminated when rut depth reached 1.5 cm or when 20,500 cycles were reached. Overall, it was noted that nearly all tests resulted in surface cracks, regardless of temperature and mix characteristics. The number of wheel passes to produce the first crack (nf) and the total number of wheel passes (nt) are presented in Table 2. Figure 2 shows the condition of the surface of some of the samples at the end of the test. The following sections summarize the effect on TDC of each of the analyzed factors.

Temperature Effect

Temperature had a major effect on TDC initiation, as can be seen by comparing nf values (Table 2). The number of wheel passes corresponding to the first crack greatly decreased with increasing temperature. Figures 2*a*, 2*b*, and 2*c* show the final surface condition of the three slabs tested at 30°C, 40°C, and 50°C.

TABLE 2 Number of Wheel Passes

Slab Number	Temperature	nf	nt
1	50°C	500	2,880
2	50°C	645	6,868
3	50°C	344	1,763
4	50°C	860	4,042
5	50°C	—	5,917
6	50°C	860	7,614
7	50°C	1,300	10,000
9	50°C	860	4,200
13	50°C	650	2,947
16	50°C	2,150	10,300
17	50°C	9,800	10,274
10	40°C	6,250	12,550
12	40°C	1,075	10,000
15	40°C	1,075	10,000
8	30°C	7,700	19,318
11	30°C	> 16,500	19,136
14	30°C	> 10,000	16,063

Void Content Effect

Results from Slabs 1, 6, and 9, tested at 50°C, demonstrate that high void content accelerates TDC initiation (Figure 2*d*). The number of wheel passes corresponding to the first crack decreased with increasing void content, and the number of cracks increased with increasing void content. Tests performed at 30°C (e.g., Slabs 8 and 11) and 40°C (e.g., Slabs 10 and 12) first showed surface changes in slabs exhibiting higher void content.

Grading Type Effect

The effect of aggregate gradation was less pronounced than the effect of temperature and void content. Nevertheless, it was observed that the coarse gradation resulted in earlier TDC initiation than did fine gradation. TDC tended to initiate at the interface between coarse aggregates and binder, especially at higher test temperatures. Particularly at 40°C, coarse aggregates appear to disturb mixture rearrangement due to compaction, which results in cracking.

Binder Content Effect

The binder content of Slabs 2, 3, and 7 was 5.8%, 7.3%, and 5.3%, respectively. Slab 7 showed little evidence of TDC, and Slab 3 showed no evidence of TDC at all. However, Slab 2, which had the optimum binder content, exhibited a significant amount of TDC at the end of the test. Despite that, the actual depth of the cracks was similar in Slabs 7 and 2, that is, 7 mm and 10 mm, respectively. That means that reduced binder content increases the time to the first crack; however, in-depth cracking progression is faster.

Segregation Effect

Field cores extracted during the forensic part of the work showed coarse aggregates at the top and fine aggregates in the lower part of the wearing course. That was replicated in simulating segregation in the laboratory-prepared slabs. For the test performed at 50°C, it was noticed that cracks were confined to the coarse-graded surface and did not progress to the lower, finer-grained layer. However, the coarse-graded aggregate at the top reduced rutting, which likely influenced TDC (Figure 2*f*).

Binder Type Effect

Slab 16 was produced with 35/50 penetration binder. This slab exhibited a significantly higher number of load passes to TDC initiation, compared with the 50/70 penetration binder, as is evident when nf values for otherwise similar slabs tested at 50°C (e.g., Slab 6) are compared.

Aggregate–Binder Adhesion Effect

It was noticed that TDC first initiated around coarse aggregates, which may be the result of poor adhesion between aggregate and binder. Hence, improving adhesion should mitigate the problem. For that purpose, an antistripping additive was used. As a result, crack opening tendency and rutting were reduced.

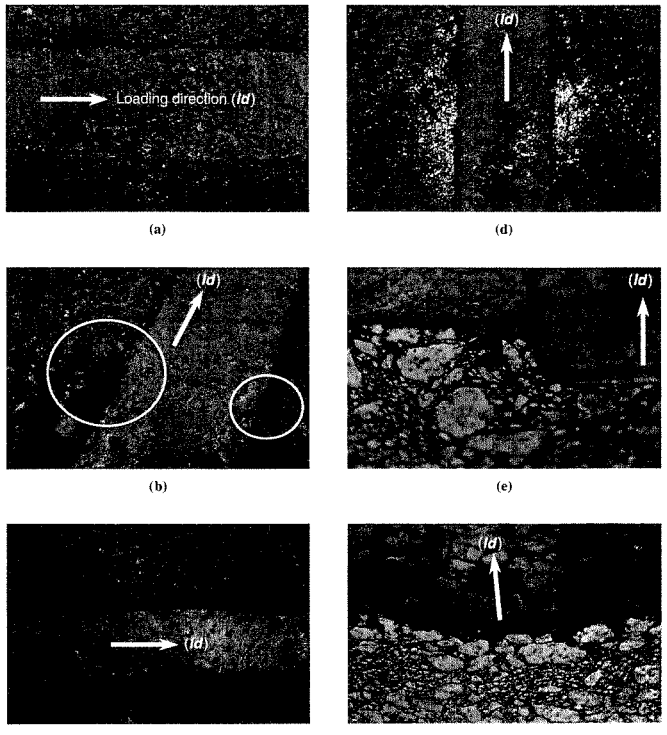

FIGURE 2 Condition of slabs after wheel-tracking test: (*a*) Slab 8, 30°C, nt = 19,318 (plan view); (*b*) Slab 10, 40°C, nt = 12,550 (plan view); (*c*) Slab 2, 50°C, nt = 6,868 (plan view); (*d*) Slab 1, 50°C, nt = 2,880 (plan view); (*e*) Slab 7, 50°C, nt = 10,000 (side view); and (*f*) Slab 17, 50°C, nt = 10,274 (side view).

NUMERICAL SIMULATION

The laboratory experiment did provide an insight into the factors affecting TDC initiation; it was concluded that TDC is often associated with rutting. To further study the interaction between these two distresses, a numerical simulation was additionally undertaken in this study. It involved a 3-D nonlinear dynamic finite element model to simulate the wheel-tracking device. The finite element program used was DIANA (*15*). The model geometry and the material characterization for this simulation are described below.

Model Geometry Characterization

The 3-D model dimensions were 30.0 × 15.0 × 7.0 cm (i.e., half test slab was analyzed because of symmetry). Twenty-node solid brick elements and rigid supports were used. Two meshes were used, one for the nonrutted surface and another for the rutted surface. The nonrutted mesh is made up of 378 elements and 2,169 nodes; the rutted mesh is made up of 468 elements and 2,600 nodes. Mesh base nodes were fixed in all directions; the lateral nodes were fixed only in the direction perpendicular to the boundary plane. Symmetry boundary plane nodes were fixed in the same way as the lateral nodes. Figure 3 shows the adopted mesh for the nonrutted geometry, as well as the loading configuration. Four sequential centered loading positions were considered. Each position was loaded with a pressure of 627 kPa in eight time steps of 0.01455 s. The loaded area was equal to the contact area of the wheel-tracking device wheel (i.e., 2.2 × 5.0/2 cm).

Material Characterization

Asphalt concrete models included a Burger's model to describe viscoelastic behavior and a constant stress cutoff smeared model to describe

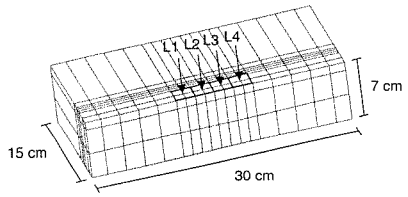

FIGURE 3 Adopted mesh.

cracking behavior. Material constants for these models were established through additional laboratory testing, as described below and summarized in Table 3.

Stiffness Modulus

Four-point bending tests were performed to measure the stiffness modulus at 30°C and 40°C. It was also possible to test two specimens at 50°C. Specimens 38.0 × 6.5 × 5.0 cm in size were extracted from each slab and submitted to sinusoidal loading, corresponding to a maximum strain at the base of 100 microstrains. This was carried out in the following decreasing order of frequency, namely, 10, 5, 2, 1, 0.5, 0.2, and 0.1 Hz. Figure 4 shows the stiffness modulus and phase angle results.

As expected, the stiffness was lower and the phase angle was high with increasing test temperatures. No difference due to the simulated construction variability was found in the three temperature groups.

Shear Modulus

An SST apparatus was used to determine the shear modulus at constant height, at temperatures of 30°C, 40°C, and 50°C. Two specimens with a 50-mm radius and 50-mm height were extracted from each slab and submitted to sinusoidal loading resulting in a shear strain amplitude of 100 microstrains, in the following decreasing order of frequency, namely, 10, 5, 2, 1, 0.5, 0.2, 0.1, 0.05, 0.02, and 0.01 Hz. Figure 5 shows the shear modulus and phase angle results. The nonlinear relationship between the logarithm of shear modulus and loading frequency, as well as between the logarithm of phase angle and loading frequency, is evident. At 30°C and 40°C the coarse- and the fine-graded mixtures possessed lower shear moduli compared with the other gradations. However, at 50°C, the mixture with Aggregate Gradation C (i.e., Slab 5) and B (i.e., Slab 4) possessed the lower moduli. At 50°C the use of harder binder and the coarser aggregate resulted in higher shear modulus. The additive did not appear to affect the shear modulus.

TABLE 3 Properties Adopted in FEM Simulation

Temperature (°C)	E1 (MPa)	E2 (MPa)	η1 (MPa.s)	η2 (MPa.s)	μ	σ_t (MPa)
30	2,100	400	50,000	130	0.35	0.50
40	500	300	16,000	85	0.40	0.25
50	200	300	6,800	80	0.48	0.15

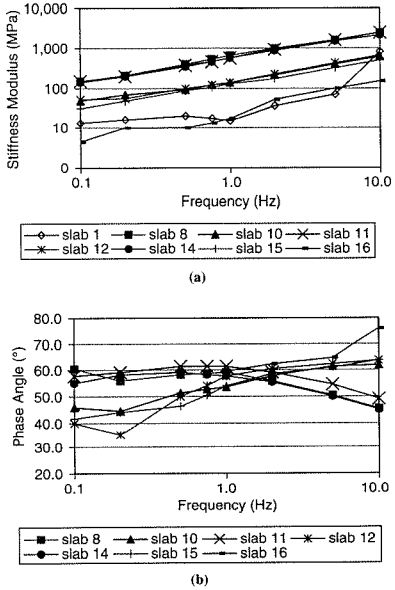

FIGURE 4 Test results: (a) stiffness modulus and (b) phase angle.

Tensile Strength

The literature suggests that the indirect tension test is suitable for quantifying cracking behavior (*16, 17*). This test was carried out by applying a compressive diametral load to a cylindrical specimen with a 50.05-mm radius and a 50.00-mm height at a controlled deformation rate of 51.00 mm per minute. Test temperature was 30°C, 40°C, and 50°C according to Table 1. Load and deflection were measured. With the use of this information, the tensile strength, as well as the fracture energy and the modulus, were determined (Table 4). Because of the high testing temperatures, the mixture responses were slightly nonlinear before the maximum load was reached. Nevertheless, fracture energy (fracture energy_{Lmax}) was computed as the triangular area of the linear approximation of the stress versus deflection diagram. In regard to tensile strength, similar values were obtained for all mixtures tested at the same temperature. The only exceptions were Slabs 7 and 16, which yielded different strengths as a result of the different binder grades used. In regard to fracture energy, low values were found in high air void mixtures (i.e., Slabs 1, 7, and 17) and vice versa (i.e., Slabs 3, 4, and 5).

Cyclic Compression Test

Cyclic compression tests were conducted to simulate traffic loading. They were carried out on cylindrical specimens (100-mm diameter and 70-mm height) at 30°C, 40°C, and 50°C and placed between two parallel loading platens. Each specimen was subjected to a 100 kPa cyclic axial square-pulse vertical stress at frequency of 0.5 Hz for 2 h.

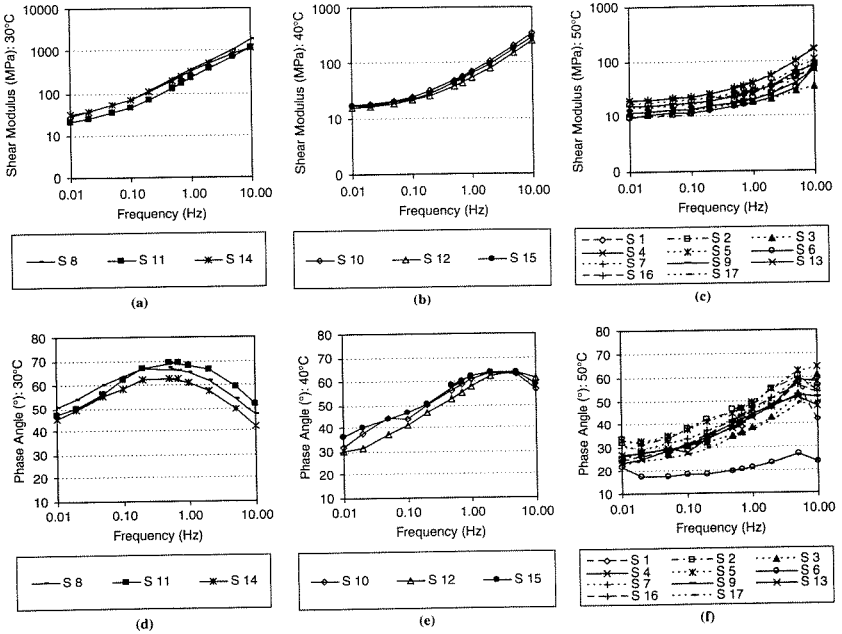

FIGURE 5 Test results: (a)–(c) shear modulus and (d)–(f) phase angle.

TABLE 4 Summary of Results Obtained by Tensile Stress Tests

Slab Number	Temperature (°C)	Load_{max} (N)	Stress (MPa)	Deflection_{Lmax} (mm)	$\text{Fracture Energy}_{Lmax}$ (MPa × mm)	Modulus (MPa)
8	30	3839	0.501	2.8	0.704	17.832
11	30	3807	0.487	4.0	0.974	12.173
14	30	3578	0.467	3.3	0.775	14.067
10	40	1926	0.259	2.4	0.312	10.741
12	40	1662	0.218	3.8	0.411	5.777
15	40	1853	0.248	2.2	0.270	11.375
1	50	924	0.119	2.2	0.129	5.491
2	50	1030	0.132	2.4	0.159	5.443
3	50	888	0.117	5.4	0.318	2.151
4	50	1049	0.139	5.8	0.401	2.398
5	50	1016	0.132	4.8	0.319	2.723
6	50	1042	0.136	3.8	0.256	3.606
7	50	1223	0.157	2.8	0.218	5.671
9	50	1088	0.140	3.7	0.257	3.798
13	50	996	0.128	3.7	0.235	3.476
16	50	1637	0.209	3.6	0.377	5.815
17	50	1073	0.139	3.6	0.250	3.859

No preload or confinement pressure was applied. During the test, plastic and elastic axial deformations were measured at specified numbers of load applications.

These data were used to adjust the mixture's viscoelastic properties using a Burger's model. The linear part of the deflection–time curve was used to establish η_1 according to Equation 1. The remaining parameters were obtained in each loading cycle by adjusting Burger's theoretical time–deflection curve to adjust the laboratory curves better. Table 5 lists the mechanical constants adjusted to the cyclic compression data tested.

$$\eta_1 = \frac{\int_{t_0}^{t_1} \sigma(t)dt}{\Delta\epsilon_{plastic}(t_0, t_1)} \quad (1)$$

where

η_1 = Maxwell's dashpot constant,
$\sigma(t)$ = applied tension, and
$\Delta\epsilon_{plastic}$ = plastic deformation difference between time t_0 and t_1.

Important differences were found in the η_1 parameter between cores of the same slab and between slabs, because of the temperature effect. In general, results were according to those obtained by other authors. For the finite element analysis, the Burger's model parameters adopted were the average values obtained for each temperature tested. These constants were frequency-shifted to model frequencies other than those tested.

Results of Numerical Simulation

Analysis of Temperature Effect

TDC takes place when a conjunction of shear and normal stresses reaches a critical combination. Cracking can originate at or near the surface of the slab. Normal stresses were found to be predictably similar for the three temperatures simulated, whereas shear stresses appeared to increase with temperature. At 50°C shear stresses appeared to exceed normal stresses in the vicinity of the load. Figure 6 shows the stress distribution as well as the cracking generated when the wheel load is in Position 4. In Positions 1, 2, and 3 the shear stresses are seen to be higher than the normal tensile stresses. It is concluded that viscoelastic behavior plays an important role in TDC initiation.

Analysis of Rutting Effect

As pointed out earlier the rutted pavement surface was modeled by reducing the slab thickness in the wheel path by 5 mm. As a result, the stress distribution changed significantly in the vicinity of the wheelpath, surpassing its tensile strength at 40°C and 50°C. At 30°C and 40°C, shear stresses remained relatively constant, whereas at 50°C they increased significantly (Figure 7). That explains why cracks were generated at 40°C after a few more wheel passes. It is concluded that the stresses generated in response to the rutted geometry can be sufficient to initiate TDC at temperatures lower than those for a nonrutted geometry.

CONCLUSIONS

The work presented in this paper summarizes the results of a laboratory and modeling study of TDC initiation. The laboratory work involved wheel-tracking tests of 17 mixtures that simulated the range of mixture characteristics established from an earlier forensic TDC study. These slabs were tested at three temperatures (30°C, 40°C, and 50°C). It was found that surface cracking initiated earlier at higher temperatures. The most important factors affecting TDC initiation were air voids (high air voids) and aggregate gradation (coarse aggregates).

TABLE 5 Burger's Model Parameters

Slab Number	E1 (MPa)		E2 (MPa)		η1 (MPa.s)		η2 (MPa.s)	
	A	B	A	B	A	B	A	B
1	99	130	270	476	1,315	6,427	69	118
2	137	133	446	365	5,863	4,079	116	90
3	—	—	—	—	—	—	—	—
4	131	131	344	325	6,276	5,285	104	97
5	131	118	395	330	10,342	7,692	100	93
6	167	236	232	300	15,603	8,758	55	59
7	120	111	348	411	5,553	4,813	86	96
8	183	220	356	430	46,203	52,371	123	146
9	123	133	245	408	18,796	4,355	89	120
10	146	147	232	345	16,212	13,061	77	103
11	—	213	—	498	—	24,202	—	159
12	165	155	279	265	16,444	20,667	78	75
13	123	—	351	—	3,249	—	95	—
14	208	135	390	193	42,455	64,964	124	77
15	143	164	317	289	11,369	15,970	96	83
16	141	144	405	288	13,675	8,063	98	97
17	131	116	299	289	8,121	5,062	84	82

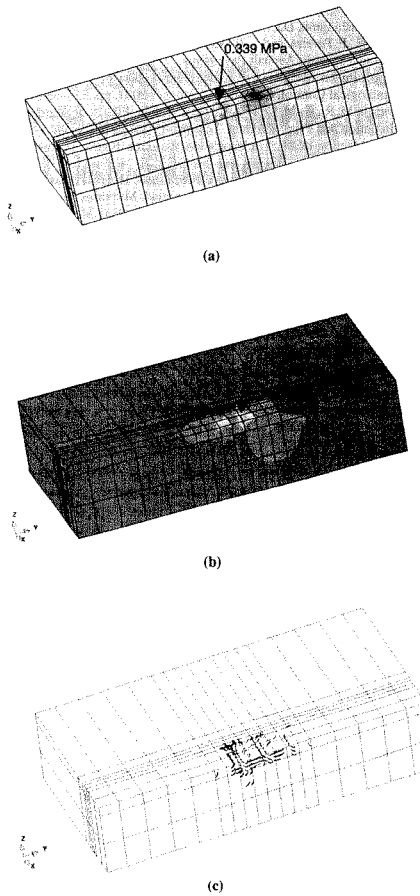

FIGURE 6 Stresses and total cracking generated in Loading Position 4 (50°C): (*a*) maximum principal stress (P1), (*b*) maximum shear stress (Q1), and (*c*) cracking.

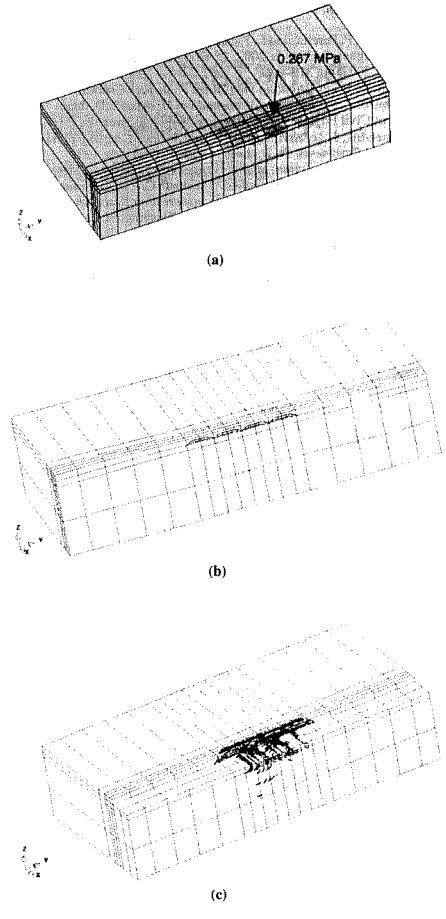

FIGURE 7 Stresses and cracking due to rutting in Loading Position 4: (*a*) maximum principal stress (P1), T = 40°C (view near wheel track edge); (*b*) cracking, T = 40°C (view near wheel track edge); and (*c*) cracking, T = 50°C.

Modeling involved a 3-D nonlinear viscoelastic finite element model, which accounted explicitly for the nonrutted and the rutted shape of the pavement surface. Modeling of the TDC involved laboratory testing to establish the viscoelastic and tensile strength properties of the asphalt mixtures tested. It was found that the rutted surface appears to contribute significantly to TDC initiation. The results provided a general vision of TDC initiation causes that may be used as guidelines in more specific research, which should consider a larger number of mixtures and samples to enable the establishment of TDC behavior models.

REFERENCES

1. Komoriya, K., T. Yoshida, and H. Nitta. "WA-DA-CHI-WA-RE" Surface Longitudinal Cracks on Asphalt Concrete Pavement. Presented at 80th Annual Meeting of the Transportation Research Board, Washington, D.C., 2001.
2. Myers, L. A. *Development and Propagation of Surface Initiated Longitudinal Wheel Path Cracks in Flexible Highway Pavements*. Ph.D. thesis. University of Florida, 2000.
3. Matsuno, S., and T. Nishizawa. Mechanism of Longitudinal Surface Cracking in Asphalt Pavement. *7th International Conference on Asphalt*

Pavements, Vol. 2, University of Nottingham, United Kingdom, 1992, pp. 277–291.
4. Freitas, E., P. Pereira, and L. Picado-Santos. *Top-Down Cracking Study* (in Portuguese). Estrada 2002. 2° Congresso Rodoviário Português. Lisboa, 2002, pp. 319–330.
5. Merrill, D. B. *Investigating the Causes of Surface Cracking in Flexible Pavements Using Improved Mathematical Models.* Ph.D. thesis. Department of Civil Engineering. University of Wales, Swansea, 2000.
6. Groenendijk, J. *Accelerated Testing and Surface Cracking of Asphaltic Concrete Pavements.* Ph.D. thesis. Delft, Netherlands, 1998.
7. Myers, L. A., R. Roque, and B. Birgisson. Propagation Mechanisms for Surface-Initiated Longitudinal Wheelpath Cracks. In *Transportation Research Record: Journal of the Transportation Research Board, No. 1778,* TRB, National Research Council, Washington, D.C., 2001, pp. 113–122.
8. Uchida K., T. Kurokawa, K. Himeno, and T. Nishizawa. Healing Characteristics of Asphalt Mixture Under High Temperature Conditions. *9th International Conference on Asphalt Pavements* (CD-ROM), Copenhagen, Denmark, 2002.
9. Uhlmeyer, J. S., K. Willoughby, L. M. Pierce, and J. P. Mahoney. Top-Down Cracking in Washington State Asphalt Concrete Wearing Courses. Issues in Pavement Design and Rehabilitation. In *Transportation Research Record: Journal of the Transportation Research Board, No. 1730,* TRB, National Research Council, Washington, D.C., 2000, pp. 110–116.
10. Svasdisant, T., M. G. Schorsch, Y. Baladi, and S. Pinyosunun. Mechanistic Analysis of Top-Down Cracking in Asphalt Pavements. In *Transportation Research Record: Journal of the Transportation Research Board, No. 1809,* Transportation Research Board of the National Academies, Washington, D.C., 2002, pp. 126–136.
11. Freitas, E., P. Pereira, and L. Picado-Santos. Assessment of Top-Down Cracking Causes in Asphalt Pavements. Presented at 3rd International Symposium on Maintenance and Rehabilitation of Pavements and Technological Control, Guimarães, Portugal, 2003, pp. 555–564.
12. Schorsch, M. R., C.-M. Chang, and G. Y. Baladi. Effects of Segregation on Initiation and Propagation of Top-Down Cracks. Presented at 82nd Annual Meeting of the Transportation Research Board, Washington, D.C., 2003.
13. Duriez M. *Traité de Materiaux de Construction.* Dunot, Paris, 1950.
14. Wang, L., L. A. Myers, and L. N. Mohammad. Micromechanics Study on Top-Down Cracking. Presented at 82nd Annual Meeting of the Transportation Research Board, Washington, D.C., 2003.
15. *DIANA Online Users Manual,* Release 8.1. TNO Building and Construction Research. Delft, Netherlands, 2003.
16. Roque, R., and W. Buttlar. The Development of a Measurement and Analysis System to Accurately Determine Asphalt Concrete Properties Using the Indirect Tensile Mode. *Journal of the Association of Asphalt Paving Technologists,* Vol. 61, 1992, pp. 304–332.
17. Martinez, F., and S. Angelone. Determination of Fracture Parameters of Asphalt Mixes by the Repeated Indirect Tensile Test. Presented at 6th RILEM Symposium, Zurich, Switzerland, 2003, pp. 387–393.

The Characteristics of Bituminous Paving Mixtures to Meet Structural Requirements Committee sponsored publication of this paper.